AGU PUBLICATIONS

Geophysical Research Letters

RESEARCH LETTER
10.1002/2014GL061155

**Key Points:**
- Antarctic fiber-optic moorings for distributed temperature sensing
- Observations of basal melting at the ice-ocean interface
- Measurement of seasonal basal melting from distributed temperature sensing moorings

**Supporting Information:**
- Readme
- Text S1

**Correspondence to:**
Scott W. Tyler,
styler@unr.edu

**Citation:**
Kobs, S., D. M. Holland, V. Zagorodnov, A. Stern, and S. W. Tyler (2014), Novel monitoring of Antarctic ice shelf basal melting using a fiber-optic distributed temperature sensing mooring, *Geophys. Res. Lett.*, *41*, 6779–6786, doi:10.1002/2014GL061155.

Received 8 JUL 2014
Accepted 4 SEP 2014
Accepted article online 8 SEP 2014
Published online 10 OCT 2014

# Novel monitoring of Antarctic ice shelf basal melting using a fiber-optic distributed temperature sensing mooring

**Scott Kobs[1], David M. Holland[2], Victor Zagorodnov[3], Alon Stern[2], and Scott W. Tyler[1]**

[1]Department of Geological Sciences and Engineering, University of Nevada, Reno, Reno, Nevada, USA, [2]Courant Institute of Mathematical Sciences, New York University, New York, New York, USA, [3]Byrd Polar Research Center, Ohio State University, Columbus, Ohio, USA

**Abstract** Measuring basal melting of ice shelves is challenging and represents a critical component toward understanding ocean-ice interactions and climate change. In November 2011, moorings containing fiber-optic cables for distributed temperature sensing (DTS) were installed through the McMurdo Ice Shelf, Antarctica, (~200 m) and extending ~600 m into the ice shelf cavity. The high spatial resolution of DTS allows for transient monitoring of the thermal gradient within the ice shelf. The gradient near the ice-ocean interface is extrapolated to the in situ freezing temperature in order to continuously track the ice-ocean interface. Seasonal melt rates are calculated to be ~1.0 mm $d^{-1}$ and 8.6 mm $d^{-1}$, and maximum melting corresponds to the arrival of seasonal warm surface water in the ice shelf cavity between January and April. The development of continuous, surface-based techniques for measuring basal melting represents a significant advance in monitoring ice shelf stability and ice-ocean interactions.

## 1. Introduction

Ice shelf stability is strongly influenced by ocean circulation within ice shelf cavities, and therefore, observations of ice shelf and cavity heat transfer, basal melting, and ocean circulation are important for assessing changes in stability resulting from climate change or other environmental factors [e.g., *Jacobs et al.*, 1992; *Jenkins et al.*, 2010b; *Robinson et al.*, 2010; *Arzeno et al.*, 2014]. The dynamics of ice-ocean interactions at the base of ice shelves are complex [*Holland and Jenkins*, 1999] and are driven by seasonal and long-term variations of ocean water temperature, salinity, and currents. Yet measurements of basal mass loss (melting) are difficult because of logistical and technical limitations of measurements over space and time. Direct high-resolution monitoring can facilitate the understanding of ice shelf mass balance in relation to local and global climatic trends [*Stanton et al.*, 2013]. Measurements of ice-ocean interactions began with ice shelf temperature measurements [*Wexler*, 1960; *Crary*, 1961] and have now evolved into a wide range of both in situ and remote sensing approaches including casts and moorings [*Jacobs et al.*, 1979; *Smethie and Jacobs*, 2005; *Robinson et al.*, 2010; *Hattermann et al.*, 2012], radar [*Corr et al.*, 2002; *Stanton et al.*, 2013], GPS [*Arzeno et al.*, 2014], downhole and robotic oceanographic instrumentation [*Jenkins et al.*, 2010a; *Stanton et al.*, 2013], and satellite altimetry [*Horgan et al.*, 2011; *Pritchard et al.*, 2012]. Each approach captures data on different spatial and temporal scales; however, continuous measurement of the ocean water column and the ice-ocean interface remains a challenge.

Ice shelf temperature profiles have long been used to estimate basal melting [*Wexler*, 1960; *Crary*, 1961] and accumulation rates [*MacAyeal and Thomas*, 1979; *Budd et al.*, 1982; *Craven et al.*, 2004]. Additionally, thermal gradients near the ice-ocean interface have been used to estimate heat flux across the interface [*Clough and Hansen*, 1979]. In most previous studies, temperature measurements typically consisted of single "point-in-time" thermal profiles, from a limited number of in situ temperature sensors. Up to now, analyses of these thermal profiles within the ice shelf have generally been limited to steady state solutions yielding mean basal melt rates. *Holland and Jenkins* [1999] summarize these heat transfer mechanisms across the ice-ocean interface with an emphasis on understanding the salinity and heat transfer mechanisms during ice shelf melting.

Distributed temperature sensing (DTS) monitoring represents a new and robust technique to monitor in situ ice shelf and ocean temperatures without the need for submerged or downhole electronics. Recent work [*Warner et al.*, 2012; *Stern et al.*, 2013; *Tyler et al.*, 2013] has demonstrated the viability and value of fiber-based temperature sensing in polar ice and oceans. In this work, we first present 14 months of calibrated ocean and

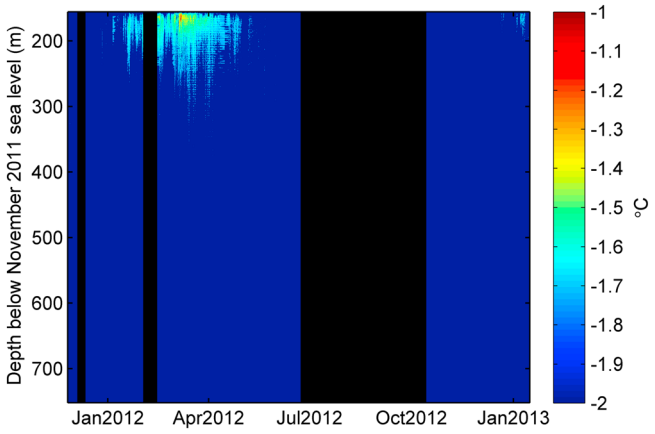


**Figure 1.** Conservative temperature (°C) recorded from Mooring BH2 at Windless Bight from November 2011 through January 2013. Distances are reported as depth below the sea level in November 2011 at the time of installation. The three longest data gaps are shown in black and are due to intermittent power failures of the surface instrumentation.

ice temperature data and develop a new method to resolve seasonal basal melt rates from changes in the thermal gradient at the ice-ocean interface.

## 2. Methods

In November 2011, two moorings (BH1 and BH2) were installed at the Windless Bright site located at 77°46.550'S, 167°32.400'E. Windless Bight is on the McMurdo Ice Shelf, adjacent to the Ross Ice Shelf [*McCrae*, 1984]. The moorings were designed primarily as a test bed for the development of both DTS [*Tyler et al.*, 2013] and novel drilling methods [*Zagorodnov et al.*, 2014]. Mooring BH1 was used primarily for testing drilling and installation methods. Mooring BH2 was completed approximately 40 m east and extends through 192.8 ± 0.025 m of ice shelf and an additional 598 m into the ocean below. At the time of drilling in November 2011, sea level was measured 37.5 m below the ice shelf surface.

The moorings and instrumentation are described in greater detail in *Tyler et al.* [2013] and *Zagorodnov et al.* [2014]. *Stern et al.* [2013] utilized preliminary data to constrain ocean circulation simulations for the first 7 months of the mooring and modeled seasonal melting. During the initial 7 month period, warm Ross Sea surface waters were observed to enter the ice shelf cavity for several months before beginning to retreat in late March 2012 as reported in *Tyler et al.* [2013] and *Stern et al.* [2013]. The moorings continued to operate through mid-January 2013 when the surface instrumentation was removed.

DTS systems record Raman backscattered photons and independent temperature sensors are employed to calibrate the backscatter signal [*Hausner et al.*, 2011]. The data from mooring BH2 were calibrated in two sections to accommodate the different ranges of temperature (ice shelf, −2 to −25°C and ocean, −1 to −2°C) and to improve the calibration using the most relevant independent temperature sensors. Unlike in *Tyler et al.* [2013], in this work we utilized additional independent temperature sensors located in the firn to constrain the calibration of the ice shelf data set over the entire deployment period. The sensors located in the firn were constructed and calibrated in the field leading to a reduced accuracy of the calibrated temperatures of the ice shelf. A dynamic three-point calibration algorithm [*Hausner et al.*, 2011] was used for the ocean data set, similar to that reported by *Tyler et al.* [2013]. Within the ice shelf, a hybrid two/three-point calibration was used. Data prior to April 2012 were used to determine a fixed value for the gain parameter ($\gamma$), and a two-point calibration was subsequently used for the entire ice shelf data set.

DTS systems report distance based on optical travel time. For the mooring cables used at Windless Bight, the optical path length is ~0.1% longer than the true physical distance, and all DTS distances have been corrected to represent true physical distances along the mooring cable. For simplicity, all depths are referenced to either the ice shelf surface (37.5 m distance above sea level) or sea level at the time of installation in November 2011. True depth below the ice shelf surface at any later point in time is controlled by both surface accumulation and basal melt.

## 3. Results

### 3.1. Ocean Thermal Profiles

Figure 1 shows the 14 month time series of calibrated ocean temperatures from mooring BH2. Conservative temperatures were calculated by methods outlined by the Thermodynamic Equation of Seawater 2010 [*McDougall and Barker*, 2011]. Calculations are made under the assumption of a uniform salinity of 34.5 practical salinity unit (psu), representative of the deep water column [*Robinson et al.*, 2010] and linear interpolation of pressure between the transducers installed along the moorings. The thermal signature of the

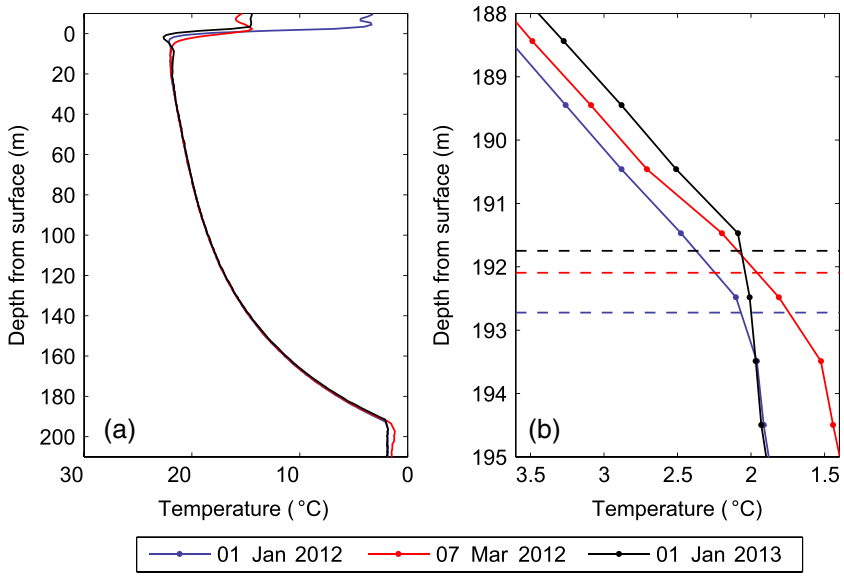


**Figure 2.** Three thermal profiles of the ice shelf before, during, and after the intrusion of warm water. (a) The transition into the ice shelf cavity is seen by the break in slope at ~200 m. (b) An expanded view close to the bottom of the ice shelf, where the transition to the ocean below is more clearly visible and changes through the year. Dashed lines represent the estimated ice draft location for each given trace.

summer warm water from the Ross Sea is observed at this location in the cavity in January of 2012 and again in January 2013. The system was removed prior to the full onset of warming in 2013; however, the initial warming is evident. The instruments ability to capture the start of the warm water intrusion in 2013 demonstrates its long-term functionality for periods greater than 1 year.

The accuracy of the calibrated ocean temperature data is 0.055°C. The temperature resolution is 0.022°C between 86 and 101 m and 0.030°C between 770 and 785 m along the fiber (see section S1 in the supporting information for a detailed description of DTS accuracy and resolution analysis). Data gaps did occur, with the largest from 23 June to 14 October 2012, when power to the instrumentation was interrupted. Temperature profiles taken before and after this gap are uniform throughout the ocean column (at the resolution of the DTS, ~0.03°C) and appear to be at or slightly below the local surface freezing temperature [*Stern et al.*, 2013]. Over the winter season, ocean temperatures near the ice-ocean interface are below the surface freezing temperature suggesting some interaction with ice at depth, consistent with results from *Robinson et al.* [2010]. Given the current resolution of the DTS system we are unable to differentiate ocean water masses at the milliKelvin resolution for further classification of ice shelf waters.

### 3.2. Ice Shelf Thermal Profiles

Figure 2 shows three representative traces of temperature through the ice shelf before, during, and after the intrusion of warm water. The exponential form of the thermal profile within the ice shelf is consistent with basal melting [*Robin*, 1955]. Temperatures in the upper and lower portion of the ice shelf show the most changes in time, with the central core of the ice shelf remaining constant over the year as expected. From 37.5 m below the surface to the bottom of the ice shelf, the instrument cables were frozen in by seawater that had filled the initial drill borehole, while the upper 37.5 m to the ice shelf surface were open and only packed with snow at the surface. At the bottom of the ice shelf, the transition to the ocean is clearly evident at all times, with a distinct change in the thermal gradient between 191 and 194 m. The accuracy and average temperature resolution for the ice shelf is 0.3°C and 0.036°C, respectively.

## 4. Discussion

Variations in ice shelf temperatures near the interfaces of the atmosphere and the ocean record the most recent events [*MacAyeal and Thomas*, 1979]. Therefore, it is expected that annual changes in thermal profile would be present in the DTS data near the base of the ice shelf due to basal melting caused by ocean heat transport.

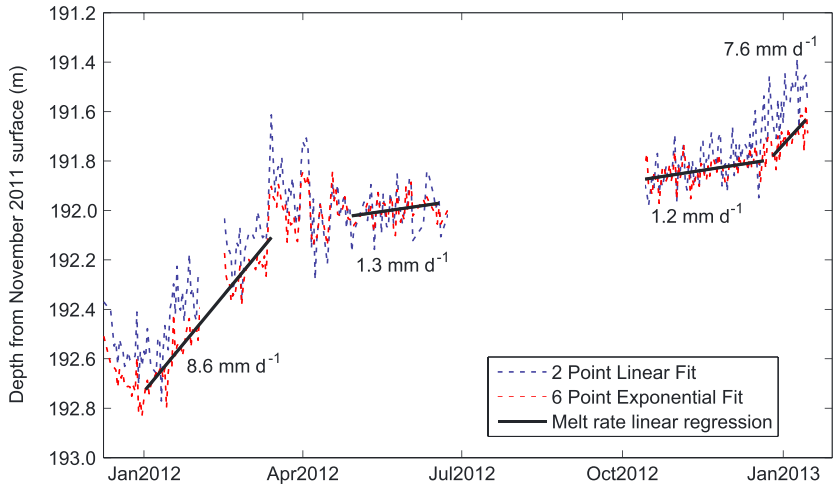


**Figure 3.** Interpolated ice-ocean interface depths based on thermal gradients within the ice shelf. Interface depths represent the daily average depth calculated from between four and eight temperature traces taken on the same day. The two-point linear fit is slightly noisier and is offset from the exponential. Daily melt rates are estimated seasonally yielding two significantly different melt rates during the Antarctic summer and winter. Melt rates are further discussed in detail in Table 1.

Figure 2b clearly shows the transition from the ice shelf to the ocean column. The transition is visible based on the DTS-measured temperatures and moves upward, particularly through the summer period of warm water intrusion. The approximate location of the ice-ocean interface can be identified in the data to within ±1 m (Figure 2b). Therefore, it is not possible to precisely calculate the basal melt because the total migration of the ice-ocean interface is less than the spatial resolution of DTS.

However, an inherent property of DTS is the ability to accurately measure the spatial variability of temperature gradients within smoothly varying profiles. From Figure 2a it is apparent that the thermal gradient near the base of the ice shelf can be approximated with high precision. Therefore, if the ocean interface temperature is known, a simple linear (or exponential) extrapolation of the ice shelf temperatures closest to the ice-ocean interface would provide a measure of the interface location. Estimation of the interface temperature is complex due to the dependence of freezing temperature on salinity at the interface [*Holland and Jenkins*, 1999] and the transient nature of heat transport upward into the ice shelf during basal melting.

As a first approximation, we assume the interface temperature to be constant in time at the in situ pressure freezing temperature (−1.99°C) for a salinity of 34.5 psu and constant pressure of 156 dbar [*Stern et al.*, 2013]. Salinity was not measured on this mooring, but the assumed salinity is consistent with previous work in the area [*Robinson et al.*, 2010]. The position of the ice-ocean interface is then calculated from the ice shelf data set by extrapolating either a linear gradient from the last two measurements in the ice shelf or a six-point exponential (consistent with the expected form of the thermal profile). As an approximation, the vertical spatial resolution of the interface can be estimated by dividing the temperature resolution (0.036°C) by the thermal gradient at the base of the ice shelf (0.38°C $m^{-1}$) and is ~0.10 m. DTS-derived temperatures represent an average over the instrument's sampling window (~1 m). For this study, the last point in the ice shelf was defined such that ~90% of the spatial sampling window of the instrument was within the ice shelf.

Figure 3 shows the inferred interface depth from the beginning of the deployment through January 2013. The calculated interface depth is noisy early in the deployment due to both data gaps and the resolution of the DTS-derived temperatures. The thermal gradient calculated by linearly fitting the closest two temperature measurements to the interface is more variable in time because of the close proximity to warming at the interface and the thermal lag time within the ice shelf. The two-point approach captures the transient heat transfer into the ice shelf more accurately during rapid melting but at a cost of greater uncertainty in the interface depth by using only two DTS-measured temperatures. The thermal lag time for one-dimensional conduction of a step change in the boundary condition temperature can be taken approximately as $z^2 \times D^{-1}$

**Table 1.** Seasonal Melt Rates Based on the Daily Average Interface Location[a]

| Date Range | Melt Rate (mm $d^{-1}$) | Melt Rate (m $yr^{-1}$) | Average Ocean Temperature at 50 m[b] (°C) | Number of Records[c] | *P* value |
|---|---|---|---|---|---|
| 2 Jan 2012 to 14 Mar 2012 | 8.6 | 3.14 | −1.74 | 57 | < 0.001 |
| 29 Apr 2012 to 18 Jun 2012 | 1.3 | 0.48 | −1.84 | 39 | 0.036 |
| 14 Oct 2012 to 21 Dec 2012 | 1.2 | 0.43 | −1.93 | 69 | < 0.001 |
| 29 Apr 2012 to 21 Dec 2012 | 0.9 | 0.34 | −1.90 | 110 | < 0.001 |
| 26 Dec 2012 to 14 Jan 2012 | 7.6 | 2.77 | −1.87 | 20 | < 0.001 |

[a]The statistical significance of each melt rate regression is evaluated using the Pearson's correlation coefficient.
[b]Based on 10 m average temperature centered 50 m (45 m to 55 m) below the ice-ocean interface.
[c]Number of traces used to evaluate the statistical significance of the regression (*P* value).

where *D* represents the thermal diffusivity of the ice and *z* represents the distance where the change would be recorded. For typical glacial ice, the thermal lag time 1 m away from a step change in temperature is ~10 days, suggesting that the calculated interface locations during periods of rapid melting may overestimate the true interface location and thereby underestimate the actual melt rate. The exponential fit, on the other hand, will dampen the transient heat transfer into the ice shelf due to the inclusion of measurements further from the interface in the fitting.

The migration of the interface location between January 2012 and early April 2012 corresponds to warm water in the ice shelf cavity (Figure 1). The net change in interface position in the first warming season (1 January to 1 May) is ~0.8 m (192.8 m to 192.0 m). Between mid-March and April, the basal elevation moves upward more quickly but then moves downward ~0.1–0.2 m before stabilizing at ~192.0 m by 1 May. This apparent "overshoot" is during the period of transition from maximum melting when the thermal gradient in the ice shelf may not be equilibrated to the melt rate.

Between 1 May 2012 and 26 December 2012, the interface position moves upward an additional ~0.2 m, implying a much smaller rate of melting corresponding to the winter period when the ocean water column is coldest and dominated by Ice Shelf Water from the Ross Ice Shelf [*Robinson et al.*, 2010]. On each side of the winter data gap (May to June and October to December), the melt rates are calculated to be ~1 mm $d^{-1}$.

Melting increases by the end of December 2012. Between late December and 15 January 2013, the interface moves ~0.15 m. The average daily melt rate for this period is 7.6 mm $d^{-1}$ and correlates with the intrusion of warm water seen in the calibrated ocean data set (Figure 1). The DTS-derived interface migrated upward from 192.76 to 191.71 m between 1 January 2012 and 1 January 2013, resulting in a cumulative melt rate of 1.05 m $yr^{-1}$ during 2012.

A further independent estimation of the basal melt rate at this location was determined by fitting the ice shelf thermal profiles to a steady state constant vertical advection and conduction model with surface accumulation [*Crary*, 1961]. Accumulation rates ~7 km northwest of the Windless Bight site are estimated to be $269 \pm 9$ kg $m^{-2}$ $yr^{-1}$ [*Kruetzmann et al.*, 2011]. The model was evaluated for the reach of fiber frozen in place and an accumulation rate of 0.25 m $yr^{-1}$ liquid water. The average modeled basal melt rate for the DTS record was $1.04 \pm 0.008$ m $yr^{-1}$, almost identical to that cumulatively measured by the DTS mooring.

Melt rates calculated by *Stern et al.* [2013] using local ocean temperatures and the turbulent transfer model of *McPhee* [2008] estimated the basal melt rate to be 0.71 m $yr^{-1}$. A change in the assumed mixed layer velocity by 0.01 m $s^{-1}$ changes the average annual melt rate by 0.1 m $yr^{-1}$ for this model. Therefore, increasing the assumed mixed layer velocity 0.03 m $s^{-1}$ would bring the estimated annual basal melt rate in line with the rate observed by tracking the ice-ocean interface by DTS.

Seasonal melt rates were determined by linear regressions of the DTS-inferred interface location over specific periods of time and are summarized in Table 1. Each period was statistically analyzed to determine the significance of the trend and melt rate. Pearson's correlation test was used to determine the significance for each time period.

This approach to calculate basal melting rates assumes the interface temperature to be constant and representative of the freezing point of the mixed layer salinity. Since the thermal gradient in the ice shelf is

nearly linear, the interface position will be linearly proportional to the assumed in situ freezing temperature. The linearized dependence of salinity on the freezing point is -5.7 × $10^{-2}$ °C $psu^{-1}$, and therefore, a difference of 1 psu in the assumed interface salinity results in a change in the freezing temperature of ~0.06°C, which is close to the reported resolution of the DTS [*Tyler et al*., 2013]. For the typical observed thermal gradient at the base of the ice shelf, a 0.06°C difference in the freezing temperature would equate to an error of ~0.07 m in the interface location.

The true position of the interface is ultimately dependent upon the assumed interface freezing temperature and therefore cannot be known precisely. However, the relative changes in the interface position are detectable independent of the accuracy of the true ice-ocean interface position. Because of the approximate linearity of freezing temperature with salinity, the choice of freezing temperature only serves to offset the true interface position, and the difference in interface position from 1 day to the next will still reflect the rate of melting. The validity of this argument does break down, however, if the actual interface salinity changes between measurements. Changes in the interface salinity in time cannot be ruled out without detailed measurements at the interface which were not available from the mooring. The assumption of constant interface salinity should be most questionable during periods of rapid basal melting and dilution of interface water or during changes in mixing with the bulk ocean waters. However, by comparing extrapolated interface locations seasonally, when the interface salinity can be expected to be similar, errors associated with changes in interface salinity can be greatly reduced.

Confidence in the measured melt rate under the assumption of constant salinity at the base of the ice shelf is further supported from measurements of the thermal gradient at the base of the ice shelf. *Holland and Jenkins* [1999] demonstrate that the thermal gradient at the base of the ice shelf during melting is expected to be amplified relative to the case without melting. This enhancement is a function of the melt rate, thermal diffusivity of ice, and the ice shelf thickness. Using average ice shelf base and surface temperatures of −2°C and −22°C, an ice shelf thickness of 192 m, representative values of thermal diffusivity and the 2011/2012 estimated melt rate of 1.05 m $yr^{-1}$, the conductive gradient (no melting) should be amplified by a factor of ~4 [*Holland and Jenkins*, 1999, equation (26)]. The conductive gradient without melting, calculated simply as the difference in surface to base temperature divided by the shelf thickness, at Windless Bight would be ~0.1°C $m^{-1}$. We would therefore expect the gradient at the interface to be enhanced to ~0.4°C $m^{-1}$. The average observed gradient over the 14 month deployment at the base of the ice shelf is 0.38°C $m^{-1}$, consistent with the value predicted for melting at the interface.

Finally, uncertainties in the interface position may also arise due to rapid changes in the basal melt rate. In the case of a melting interface, the ice shelf thermal gradient near the ice-ocean interface is continually varying in time. Under slow and steady melting, thermal conduction within the ice shelf will continually adjust the gradient. Close to the ice shelf front, the peak basal melting occurs over a short window in the Antarctic summer consistent with *Stern et al.* [2013] and *Arzeno et al.* [2014]. The temperatures measured further from the interface within the ice shelf during this period of rapid basal melting may not be in thermal equilibrium and will not yet be equilibrated to the new melt rate. The calculated gradient will be over steepened and will result in a prediction of greater basal movement than actually occurred. There is possible evidence of this behavior in Figure 3 in mid-March and April, when the ice shelf appears to thicken from ~191.9 m to ~192.1 m at a time when accumulation of frazil ice would be unlikely, although prediction of frazil ice formation is difficult. As the temperatures in the lower portion of the ice shelf relax to accommodate the smaller basal melting rates in the winter, the apparent interface location calculated from the gradient migrates back downward and stabilizes at the apparent winter basal melt rate. However, the annual melt rates, calculated by comparing basal elevations early in each summer, will be far less affected by thermal disequilibrium as the melt rate is far slower in the winter months allowing for greater confidence in estimating total annual melt over any given year period.

## 5. Conclusions

We have presented observations of ice shelf and ocean thermal profiles from surface based fiber-optic temperature sensing. Using the evolution of the thermal profile at the ice-ocean interface, the seasonal basal melting could be estimated and was clearly regulated by the ice shelf cavity water temperatures. The DTS-derived melt rate compares well with long-term average melt rates reported and modeled for the area.

This new approach provides for the first time, continuous in situ measurement of basal melting measured from surface instrumentation. Although DTS systems integrate over length scales at or larger than the anticipated annual melt rate at Windless Bight, the continuous nature of the measurement allows the gradient to be calculated with far more certainty than individual point measurements and allows for higher vertical spatial resolution of the interface. Unlike traditional thermal gradient measurements in ice shelves used to infer a yearly or average melt rate, the continuous in time temperature measurements within the ice shelf provides seasonal and annual rate estimates and also showed the maximum melting to coincide with intrusion of warm waters beneath the ice shelf.

From a practical point of view DTS allows temperature to be measured along the entire mooring and can "adapt" to the upwardly moving interface. Unlike traditional point sensors whose location is fixed in depth, the frozen cable slowly exposes itself to the interface and will provide continuous measurements at the interface. While the instrument used in this study had a 1 m sample integration, next generation DTS systems can sample at intervals of 0.1–0.2 m and will provide far better resolution of the gradient at the interface. This enhanced resolution, combined with potential advances in salinity and current sensing, will allow opportunity to explore the nature of the thermal boundary layer and melting at the ice-ocean interface.

**Acknowledgments**

Funding for this project has been provided by the Office of Polar Programs of the National Science Foundation (NSF) under grant ANT-10431154, and support was provided to V.Z. and D.M.H. by grants ANT-1043217 and ANT-1043395. The authors would like to thank the reviewers for their valuable comments and suggestions. Additional instrument support was provided by the CTEMPs facility under EAR-1128999, and engineering services were provided by the UNAVCO facility with support from the NSF and NASA under NSF Cooperative agreement EAR-0735156. The full calibrated temperature data sets from mooring BH2, along with documentation on the calibration procedures and parameters will be available at both http://efdl_5.cims.nyu.edu/dts_mcm/ and the National Snow and Ice Data Center. Conservative temperature was calculated using the Thermodynamic Equation of Seawater - 2010, Gibbs-SeaWater (GSW) Oceanographic Toolbox [*McDougall and Barker*, 2011], TEOS-10 GSWv3.01 MATLAB toolbox, www.teos-10.org/software.htm.

The Editor thanks Laurence Padman and an anonymous reviewer for their assistance in evaluating this paper.

## References

Arzeno, I. B., R. C. Beardsley, R. Limeburner, B. Owens, L. Padman, S. R. Springer, C. L. Stewart, and M. J. M. Williams (2014), Ocean variability contributing to basal melt rate near the ice front of Ross Ice Shelf, Antarctica, *J. Geophys. Res. Oceans*, *119*, 4214–4233, doi:10.1002/2014JC009792.

Budd, W. F., M. J. Corry, and T. H. Jacka (1982), Results from the Amery Ice Shelf project, *Ann. Glaciol.*, *3*, 36–41.

Clough, J. W., and B. L. Hansen (1979), The Ross Ice Shelf project, *Science*, *203*(4379), 433–434, doi:10.1126/science.203.4379.433.

Corr, H. F. J., A. Jenkins, K. W. Nicholls, and C. S. M. Doake (2002), Precise measurement of changes in ice-shelf thickness by phase-sensitive radar to determine basal melt rates, *Geophys. Res. Lett.*, *29*(8), 1232, doi:10.1029/2001GL014618.

Crary, A. P. (1961), Glaciological regime at Little America Station, Antarctica, *J. Geophys. Res.*, *66*(3), 871–878, doi:10.1029/JZ066i003p00871.

Craven, M., I. Allison, R. Brand, A. Elcheikh, J. Hunter, M. Hemer, and S. Donoghue (2004), Initial borehole results from the Amery Ice Shelf hot-water drilling project, *Ann. Glaciol.*, *39*(1), 531–539, doi:10.3189/172756404781814311.

Hattermann, T., O. A. Nøst, J. M. Lilly, and L. H. Smedsrud (2012), Two years of oceanic observations below the Fimbul Ice Shelf, Antarctica, *Geophys. Res. Lett.*, *39*, L12605, doi:10.1029/2012GL051012.

Hausner, M. B., F. Suárez, K. E. Glander, N. van de Giesen, J. S. Selker, and S. W. Tyler (2011), Calibrating single-ended fiber-optic Raman spectra distributed temperature sensing data, *Sensors (Basel)*, *11*(11), 10,859–10,879, doi:10.3390/s111110859.

Holland, D. M., and A. Jenkins (1999), Modeling thermodynamic ice-ocean interactions at the base of an ice shelf, *J. Phys. Oceanogr.*, *29*, 1787–1800, doi:10.1175/1520-0485(1999)029<1787:MTIOIA>2.0.CO;2.

Horgan, H. J., R. T. Walker, S. Anandakrishnan, and R. B. Alley (2011), Surface elevation changes at the front of the Ross Ice Shelf: Implications for basal melting, *J. Geophys. Res.*, *116*, C02005, doi:10.1029/2010JC006192.

Jacobs, S. S., A. L. Gordon, and J. L. Ardai (1979), Circulation and melting beneath the Ross Ice Shelf, *Science*, *203*(4379), 439–443, doi:10.1126/science.203.4379.439.

Jacobs, S. S., H. H. Hellmer, C. S. M. Doake, A. Jenkins, and R. M. Frolich (1992), Melting of ice shelves and the mass balance of Antarctica, *J. Glaciol.*, *38*(130), 375–387.

Jenkins, A., K. W. Nicholls, and H. F. J. Corr (2010a), Observation and parameterization of ablation at the base of Ronne Ice Shelf, Antarctica, *J. Phys. Oceanogr.*, *40*(10), 2298–2312, doi:10.1175/2010JPO4317.1.

Jenkins, A., P. Dutrieux, S. S. Jacobs, S. D. McPhail, J. R. Perrett, A. T. Webb, and D. White (2010b), Observations beneath Pine Island Glacier in West Antarctica and implications for its retreat, *Nat. Geosci.*, *3*(7), 468–472, doi:10.1038/ngeo890.

Kruetzmann, N. C., W. Rack, A. J. McDonald, and S. E. George (2011), Snow accumulation and compaction derived from GPR data near Ross Island, Antarctica, *Cryosphere*, *5*(2), 391–404, doi:10.5194/tc-5-391-2011.

MacAyeal, D. R., and R. H. Thomas (1979), Ross Ice Shelf temperatures support a history of ice-shelf thickening, *Nature*, *282*, 703–705, doi:10.1038/282703a0.

McCrae, I. R. (1984), *A Summary of Glaciological Measurements Made Between 1960 and 1984 on the McMurdo Ice Shelf, Antarctica*, Dep. of Theor. and Appl. Mech., Auckland, New Zealand.

McDougall, T. J., and P. M. Barker (2011), Getting started with TEOS-10 and the Gibbs Seawater (GSW) Oceanographic Toolbox, 28 pp., SCOR/IAPSO WG127.

McPhee, M. (2008), *Turbulent Ocean Boundary Layer Exchange Processes, Air-Ice-Ocean Interactions*, pp. 109–131, Springer, New York.

Pritchard, H. D., S. R. M. Ligtenberg, H. A. Fricker, D. G. Vaughan, M. R. van den Broeke, and L. Padman (2012), Antarctic ice-sheet loss driven by basal melting of ice shelves, *Nature*, *484*, 502–505, doi:10.1038/nature10968.

Robin, G. d. Q. (1955), Ice movement and temperature distribution in glaciers and ice sheets, *J. Glaciol.*, *18*, 523–532, doi:10.3189/002214355793702028.

Robinson, N. J., M. J. M. Williams, P. J. Barrett, and A. R. Pyne (2010), Observations of flow and ice-ocean interaction beneath the McMurdo Ice Shelf, Antarctica, *J. Geophys. Res.*, *115*, C03025, doi:10.1029/2008JC005255.

Smethie, W. M., and S. S. Jacobs (2005), Circulation and melting under the Ross Ice Shelf: Estimates from evolving CFC, salinity and temperature fields in the Ross Sea, *Deep Sea Res., Part I*, *52*(6), 959–978, doi:10.1016/j.dsr.2004.11.016.

Stanton, T. P., W. J. Shaw, M. Truffer, H. F. J. Corr, L. E. Peters, K. L. Riverman, R. Bindschadler, D. M. Holland, and S. Anandakrishnan (2013), Channelized ice melting in the ocean boundary layer beneath Pine Island Glacier, Antarctica, *Science*, *341*(6151), 1236–1239, doi:10.1126/science.1239373.

Stern, A. A., M. S. Dinniman, V. Zagorodnov, S. W. Tyler, and D. M. Holland (2013), Intrusion of warm surface water beneath the McMurdo Ice Shelf, Antarctica, *J. Geophys. Res. Oceans*, *118*, 7036–7048, doi:10.1002/2013JC008842.

Tyler, S. W., D. M. Holland, V. Zagorodnov, A. A. Stern, C. Sladek, S. Kobs, S. White, F. Suárez, and J. Bryenton (2013), Using distributed temperature sensors to monitor an Antarctic ice shelf and sub-ice-shelf cavity, *J. Glaciol.*, *59*(215), 583–591, doi:10.3189/2013JoG12J207.

Warner, R. C., M. Craven, B. Galton-Fenzi, A. Elcheikh, A. Christensen, and S. W. Vogel (2012), Distributed temperature sensing in the Amery Ice shelf and the sub ice shelf ocean, in *26th International Forum for Research Into Ice Shelf Processes*, pp. 50–51. [Available at http://rechenknecht.natgeo.su.se/FRISP2012/FRISP_Book_of_Abstracts_May22.pdf.]

Wexler, H. (1960), Heating and melting of floating ice shelves, *J. Glaciol.*, *3*(27), 626–645.

Zagorodnov, V., S. W. Tyler, D. M. Holland, A. A. Stern, L. G. Thompson, C. Sladek, S. Kobs, and J. Nicols (2014), New technique for access-borehole drilling in shelf glaciers using lightweight drills, *J. Glaciol.*, *60*(223), doi:10.3189/2014JoG13J211.